Science Bulletin 64 (2019) 904–909

Contents lists available at ScienceDirect

Science Bulletin

journal homepage: www.elsevier.com/locate/scib

Science Bulletin
www.scibull.com

Article

# Inorganic antimony halide hybrids with broad yellow emissions

Zhifang Tan [1], Manchen Hu [1], Guangda Niu *, Qingsong Hu, Jinghui Li, Meiying Leng, Liang Gao, Jiang Tang *

*Wuhan National Laboratory for Optoelectronics (WNLO) and School of Optical and Electronic Information, Huazhong University of Science and Technology, Wuhan 430074, China*

ARTICLE INFO

*Article history:*
Received 13 March 2019
Received in revised form 28 April 2019
Accepted 7 May 2019
Available online 22 May 2019

*Keywords:*
Inorganic
Perovskite variant
Lead-free
White light-emitting diodes

ABSTRACT

Lead halide perovskites exhibit unexceptionable photoelectric properties. However, these materials are unsatisfactory in terms of stability and toxicity. Herein, we report $Rb_7Sb_3Cl_{16}$ as a new kind of lead free perovskite variants. This material can be easily obtained through hydrothermal reactions. The composition is determined through structure refinement, elemental analysis and X-ray photoelectron spectra. $Rb_7Sb_3Cl_{16}$ exhibits a broad yellow emission at 560 nm, with a Stokes shift of 175 nm and a photoluminescence quantum yield (PLQY) around 26%. $Rb_7Sb_3Cl_{16}$ also shows good thermal and water stability due to its inorganic composition. White light-emitting diodes (LEDs) are constructed by combining $Rb_7Sb_3Cl_{16}$ as yellow phosphors, our previously reported $Cs_2SnCl_6$:2.75%Bi as blue phosphors, and commercial UV LED chips as the excitation source, producing a white light with the Commission Internationale de'Eclairage (CIE) color coordinates at (0.39, 0.38).



## 1. Introduction

Lead halide perovskites have recently attracted great attentions as promising next-generation light emitting materials, considering their excellent light emitting properties like high photoluminescence quantum yield (PLQY, 70%–100%), narrow full-width-at-half-maximum (FWHM, 15–40 nm), wide color gamut (~150% National Television Standards Committee (NTSC)), and low-temperature synthesis process [1–8].

Despite the above good properties, the poor stability and toxicity of lead halide perovskites still severely limit their practical applications. For example, the previously studied lead halide perovskites ($CH_3NH_3PbI_3$ and $NH_2CH=NH_2PbI_3$) are susceptible to external conditions including moisture, heat, light and electric fields etc. [9–11]. Replacing organic A sites with inorganic cations is beneficial for the stability [12]. In terms of the toxicity, lead (Pb) is accumulative in human body causing brain related symptoms, and European Commission RoHS (Restriction of the use of certain hazardous substances) regulates the use of Pb in electrical and electronic equipment <0.1%. Therefore, it is of vital importance to develop lead-free perovskites hopefully with good stability and considerable light emitting properties.

Substitution of $Pb^{2+}$ with isovalent ions ($Sn^{2+}$, $Ge^{2+}$) is expected to give good results, but the easy oxidation of these cations lead to poor stability. It has also been reported to replace two $Pb^{2+}$ with one monovalent cation B' (such as $Ag^+$) and one trivalent cation B" (such as $Bi^{3+}$, $In^{3+}$) to form $A_2B'B''X_6$ double perovskites [13,14]. Yet, the indirect or parity forbidden transitions of double perovskites generally result in poor light emitting properties, while further improvement relies on doping certain elements [15–19].

Another promising strategy is to utilize elements with different valence states, such as $Sb^{3+}$, $Bi^{3+}$ and $In^{3+}$. A significant change is that the crystal structure decreases from three-dimensional (3D) structure to lower dimensions (2D, 1D or even 0D) in order to keep charge balance. The low electronic dimensionality associated with these structures could confine the carriers and lead to high photoluminescence. According to previous theoretical studies, $Sb^{3+}$ ($5s^25p^0$) exhibits closest energy levels to $Pb^{2+}$ ($6s^26p^0$) among above trivalent cations, and thereby the produced valence band maximum and conduction band minimum of Sb-based perovskite variant are also similar to lead perovskites, which promises defect tolerance [20,21]. Besides the low-toxicity, element Sb has abundant reserves on Earth with the annual production as 53,000 tons. Overall, antimony is a promising choice to produce lead free perovskites variants. Ma and co-workers [22] reported a $(C_9NH_{20})_2SbCl_5$ hybrid perovskite with a photoluminescence quantum yield (PLQY) of 98%, which is the highest among values for both lead and lead-free perovskites. The imperfection is the poor stability due to the presence of organic A site. Thereby, it is interesting to explore other Sb halide perovskite variants with inorganic

* Corresponding authors.
*E-mail addresses:* guangda_niu@hust.edu.cn (G. Niu), jtang@mail.hust.edu.cn (J. Tang).
[1] These authors contributed equally to this work.

https://doi.org/10.1016/j.scib.2019.05.016
2095-9273/

compositions, which may simultaneously achieve high PLQY and good stability.

Herein we reported a new family of inorganic Sb-based perovskite variant—$Rb_7Sb_3Cl_{16}$, with $Rb^+$ ions at A sites. $Rb^+$ ion has a smaller ionic radius (1.52 Å) compared to $Cs^+$ (1.67 Å), and is expected to form a more compact crystal structure. $Rb_7Sb_3Cl_{16}$ could be produced through a convenient hydrothermal synthesis process. As-synthesized $Rb_7Sb_3Cl_{16}$ powder exhibits a broad, yellow emission locating at 560 nm and a PLQY value of 26%. The broad emission is probably due to the formation of self-trapped exciton (STE) upon excitation. Because of the inorganic nature, $Rb_7Sb_3Cl_{16}$ could resist thermal treatment up to 230 °C, and exhibit excellent stability toward water. Finally, we combined the yellow emitting $Rb_7Sb_3Cl_{16}$ with our previously reported blue emitting $Cs_2SnCl_6$:Bi [23], and demonstrated their use for white light emission. The assembled LED exhibited a white light emission with a correlated color temperature (CCT) of 3,986 K, and a Commission Internationale de l'Eclairage (CIE) coordinate of (0.39, 0.38).

## 2. Materials and methods

### 2.1. Materials and chemicals

Rubidium chloride (RbCl, 99.99%, Alfa Aesar, China), rubidium bromide (RbBr, Alfa Aesar, 99.99%), rubidium iodide (RbI, 99.99%, Alfa Aesar), antimony chloride ($SbCl_3$, 99.0%, Alfa Aesar), antimony bromide ($SbBr_3$, 99.0%, Alfa Aesar), antimony iodide ($SbI_3$, 99.0%, Alfa Aesar), hydrochloric acid (HCl, 37 wt% in water, Sinopharm Chemical Reagent Co., Ltd., China), hydrobromic acid (HBr, 40 wt % in water, Sinopharm Chemical Reagent Co,. Ltd.), hydroiodic acid (HI, 37 wt% in water, Sinopharm Chemical Reagent Co., Ltd.), were the precursors. All the chemicals were used without further purification, unless otherwise stated.

### 2.2. Synthesis

The 362.76 mg (3 mmol) RbCl, 145.75 mg (0.5 mmol) $SbCl_3$ powders were added in a polytetrafluoroethylene (PTFE) container with 4.0 mL of 37% hydrochloric acid. The container was placed in a muffle furnace and kept at 180 °C for 10 h. Crystals were obtained by cooling the solution down to room temperature naturally. White and transparent crystals of $Rb_7Sb_3Cl_{16}$ can be separated through immediate filtration and washed by methanol and ethyl acetate. Bromide and iodide-based materials were synthesized following the same method but using the corresponding precursors.

### 2.3. Fabrication of LED devices

White LEDs were fabricated by combining UV LED chips (365 nm, 10 W, EPISTRA), the present $Rb_7Sb_3Cl_{16}$ and another lead-free perovskite $Cs_2SnCl_6$:2.75%Bi blue phosphor. The chip was first fixed on the bottom of a reflector. These two lead-free perovskite phosphors were mixed with silicone thoroughly. And then the phosphor-silicone mixture was coated on the surface of the LED chips to produce white LEDs.

### 2.4. Measurement and characterization

Powder X-ray diffraction (PXRD) (using a Cu Kα rotating anode, D8 ADVANCE, Bruker, Germany) was used to determine the phase of the samples. MgO powder was used to calibrate before the diffuse reflectance spectra of powder samples were obtained. Edinburgh Instruments FLS 980 spectrometer, xenon lamp, Time-Correlated Single Photon Counting (TCSPC) module (diode laser excitation at $\lambda = 375$ nm), red-sensitive photomultiplier (R928) and integrating sphere were used to record the PLQY, steady-state and time-resolved PL (TRPL) spectra of the samples. X-ray photoelectron spectroscopy (XPS) spectra were obtained on AXIS Supra, with X-ray beam focusing on an area of 2 $mm^2$. Dried powders of polycrystalline samples were tested for temperature-dependent PL spectra with a temperature controller system.

### 2.5. Rietveld refinements

Rietveld refinements on powder X-ray diffraction data were carried out by employing the General Structure Analysis System software package.

## 3. Results and discussion

Since Rb-Sb-X remains rarely reported so far, we first synthesized and studied Rb-Sb-X single crystals for a better understanding of its structural and optical properties. Rb-Sb-X single crystals were grown by hydrothermal method. The precursor solution was a stoichiometric mixture of rubidium chloride and antimony chloride dissolved in HCl. The precursor was added in a PTFE container; then the container was placed in a muffle furnace setting at 180 °C for 10 h. After cooling to room temperature naturally, light yellow hexagonal crystals were obtained (Fig. S1 online). The products were filtrated and washed by methanol and ethyl acetate for three times, which removed the surface-absorbed ions and dried for further use.

The transparent Rb-Sb-Cl crystals have a hexagonal shape, and the largest crystal size is 6 mm × 4 mm × 0.8 mm (Fig. 1a). Similarly, Rb-Sb-Br and Rb-Sb-I could also be synthesized by the same method except the utilization of the corresponding rubidium and

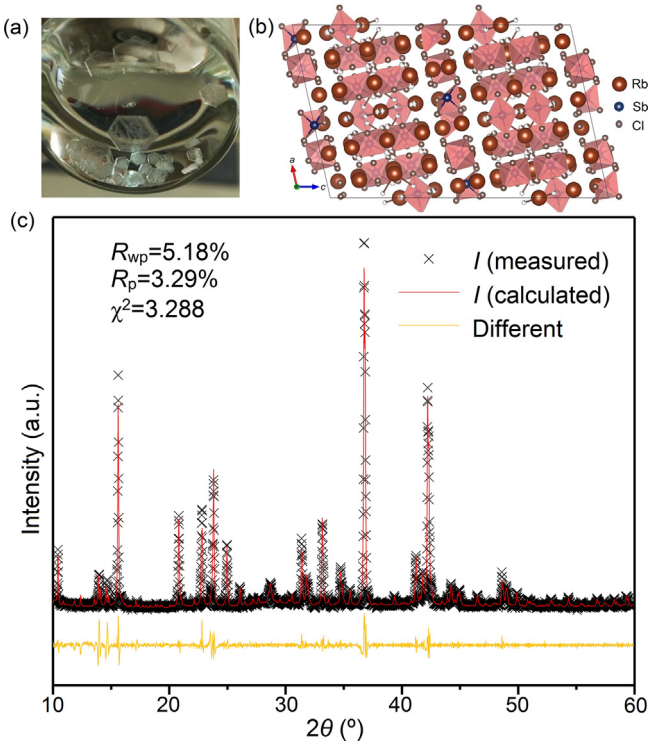


**Fig. 1.** (Color online) Sample and structure characterization of $Rb_7Sb_3Cl_{16}$. (a) The picture of $Rb_7Sb_3Cl_{16}$ crystals in HCl solution. (b) The crystal structure. (c) XRD patterns of $Rb_7Sb_3Cl_{16}$ and the related Rietveld refinement results. Crosses represent the measured results, upper lines are refinement results, under lines are the difference profile between measured and refinement results, black vertical lines represent the standard diffractions.

antimony halide, and hydrobromic (HBr) and hydroiodic (HI) acid as the solvent. The Rb-Sb-Br crystal exhibits yellow color and its edge is around 0.5 mm, while Rb-Sb-I is a big deep crimson crystal about 1 cm long (Fig. S2 online). Since bromide- and iodide-based materials have almost no fluorescence, we then focus on chloride-based perovskite variant for further characterizations and discussions. As shown in Fig. 1b, the $[SbCl_6]^{3-}$ octahedron is connected with each other by a ridge and two octahedrons form a dimer. These dimers are then separated by $Rb^+$ ions. Powder X-ray diffraction (XRD) measurement was also applied to the collected small powder crystals. Fig. 1c shows the Rietveld refinement results for $Rb_7Sb_3Cl_{16}$. The XRD pattern is in good agreement with the monoclinic crystal structure (space group: *C 2/c*) with $a = 22.255$ Å, $b = 12.849$ Å, and $c = 34.946$ Å, $\alpha = \gamma = 90°$, and $\beta = 122.6°$. The black crosses represent the measured XRD results and upper lines are the Rietveld refinement results. The as-obtained goodness-of-fit parameter $\chi^2$ is 3.288, and the reliability factors $R_{wp}$ is 5.18%, $R_p$ is 3.29% ($R_p$ represents full spectrum factor, $R_{wp}$ represents weighted full spectrum factor), demonstrating the phase purity of $Rb_7Sb_3Cl_{16}$.

XPS was carried out to further verify the composition (Figs. 2a and S3 (online)). Two distinct peaks appeared at 109.68 eV (Rb $3d_{5/2}$) and 111.16 eV (Rb $3d_{3/2}$), i.e., with a binding energy splitting of 1.48 eV, which was consistent with $Rb^+$ [24]. The two peaks at 540.27 and 530.87 eV were attributed to $Sb^{3+}$ $3d_{3/2}$ and $3d_{5/2}$, respectively. In addition, the peaks at 198.10 and 199.59 eV were attributed to $Cl^-$ $2p_{3/2}$ and $2p_{1/2}$. And the determined Rb, Sb and Cl contents are 16.98%, 7.29%, and 37.86%, respectively. The calculated atomic ratio is Rb: Sb: Cl = 7.0:3.0:15.6, which is very close to the expected ratio of 7:3:16. Then inductively coupled plasma optical emission spectrometry (ICP-OES) was used to quantitatively characterize the chemical compositions of the products. As shown in Table S1 (online), the calculated concentrations for $Rb^+$ and $Sb^{3+}$ are 0.219 and 0.093 mmol/L, respectively. The ratio of $Rb^+$ to $Sb^{3+}$ is 2.35, which is close to the stoichiometric ratio of $Rb_7Sb_3Cl_{16}$ ($Rb^+$/$Sb^{3+}$ is 2.33). From the XRD, and XPS results, we determined the samples as $Rb_7Sb_3Cl_{16}$.

Generally, hybrid halide perovskites suffer from poor thermodynamic stability with low decomposition temperatures ($T_d$) due to the presence of organic component. Here, thermogravimetric analysis (TGA) was carried out for the powder samples $Rb_7Sb_3Cl_{16}$ (Fig. 2b) to determine the thermal stability. The thermal decomposition of $Rb_7Sb_3Cl_{16}$ starts at around 230 °C, which is in agreement with the boiling point of $SbCl_3$ (228 °C). After the evaporation of antimony halide, the remaining substance is RbCl, accounting for 55% of the samples, which is also consistent with TGA results.

UV–vis absorption and PL spectroscopy were measured under ambient atmosphere in order to gain more information about the properties of $Rb_7Sb_3Cl_{16}$. The absorption spectrum of pristine $Rb_7Sb_3Cl_{16}$ (Fig. 3a) covered the main range of 300–400 nm with a peak locating at 350 nm (3.54 eV). There was also weak absorption between 400 and 600 nm (2.76 eV), which was attributed to the tail states within the products. Further improvement of the product quality to suppress such states is recommended. Ultraviolet photoelectron spectrum was used to determine the energy level of $Rb_7Sb_3Cl_{16}$ (Fig. S4 online). The Fermi level was obtained by subtracting the binding energy of the secondary electron cutoffs from the excitation energy of HeI UPS spectra. As shown in Fig. S4 (online), the Fermi level is calculated as 5.8 eV. The energy difference between valence band maximum and Fermi level is obtained from the low binding energy tails (1.5 eV). As shown in Fig. 3a, the peak of PL excitation (PLE) spectrum located at 385 nm. Notably, there is no photoluminescence with exciting wavelength larger than 400 nm, verifying that the absorption in this region is due to the defect states. The emission spectra of $Rb_7Sb_3Cl_{16}$ showed a peak at 560 nm with a broad FWHM of 100 nm. The Stokes shift was thereby calculated as 175 nm, and such large stokes shift is beneficial for applications as light emitting phosphors as it could reduce self-absorption. Such broad emission and large Stokes shift are believed to stem from self-trapped exciton emission, similar to the typically observed broad band PL in low dimensional lead halide perovskites with distorted lead halide octahedra [18,25]. For halide perovskites, photogenerated excitons often cause the transient deformation of crystal lattice due to the polarizable lattice and are thus localized, forming the so-called self-trapped exciton [18,26]. The broadband emission with large Stokes shift was caused by the nuclear coordinate changing and some energy dissipating for elastic lattice distortion [25,27]. Further improvement over the photoluminescence may rely on surface passivation and quantum dots or nanosheets structures, like introducing passivating ligands (oleic acids etc.) or synthesizing nanostructures, which could further decrease the electronic dimensionality for exciton confinement.

Time-resolved PL spectrum was measured to gain more insights into the exciton recombination dynamics. The PL decay curve can be well fitted by a single exponential function.

$$F(t) = Ae^{-\frac{t}{\tau}}F(t), \quad (1)$$

where $A$ is a constant, $\tau$ is the decay time. As shown in Fig. 3b, the PL lifetime is analyzed as 207.85 ns. Normally, the PL lifetimes of representative STE emission range from 100 to 1,000 ns. Such slow decay kinetics also verifies that STE emission is the main radiative channel.

Additionally, the temperature-dependent PL (TDPL) spectra of $Rb_7Sb_3Cl_{16}$ were obtained (Figs. 3c and S5 (online)). We chose

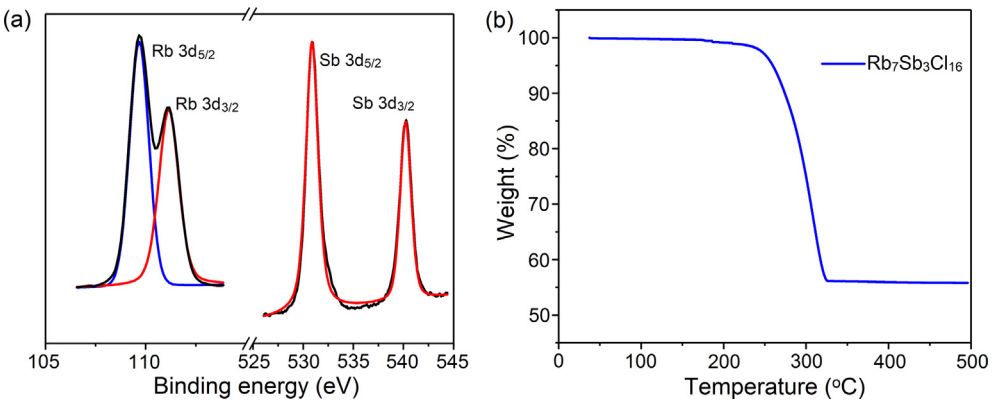


**Fig. 2.** (Color online) Elemental and thermal properties of $Rb_7Sb_3Cl_{16}$. (a) High-resolution XPS spectra and peak fitting for Rb 3d and Sb 3d respectively. (b) Thermal decomposition of $Rb_7Sb_3Cl_{16}$.

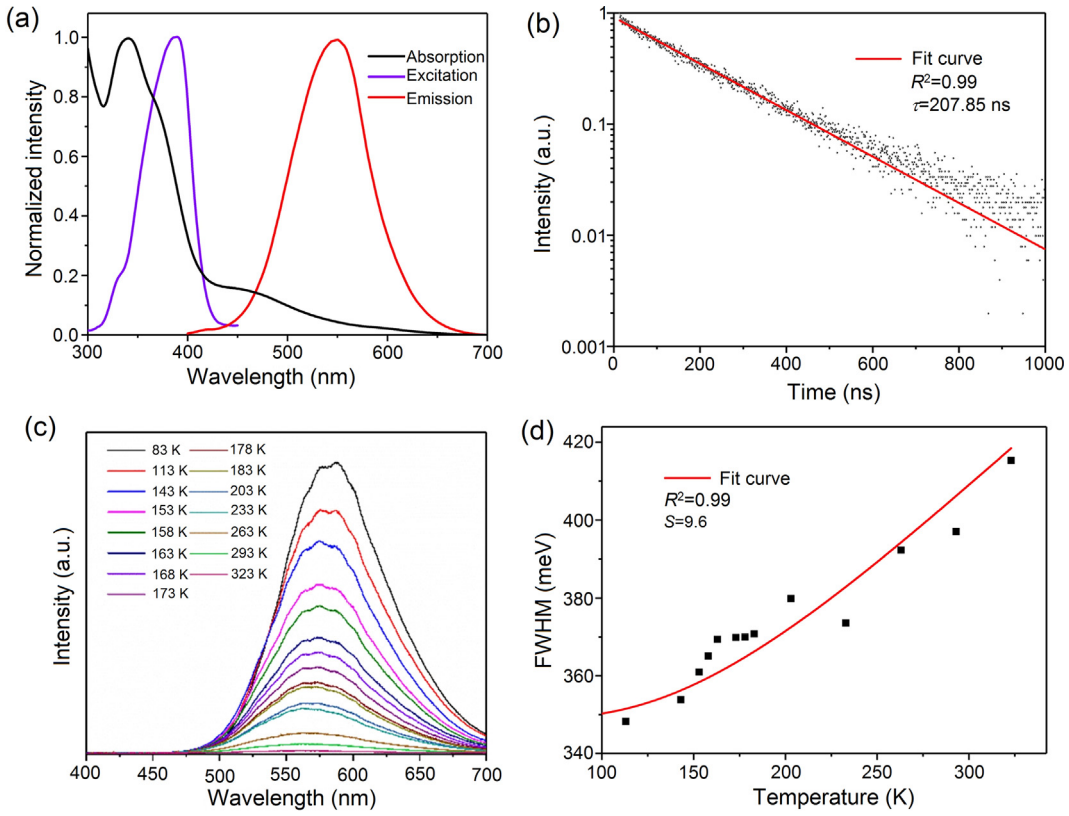


**Fig. 3.** (Color online) Photoproperties of $Rb_7Sb_3Cl_{16}$. (a) UV–vis absorption spectrum, excitation and emission spectra of $Rb_7Sb_3Cl_{16}$. (b) PL decay of $Rb_7Sb_3Cl_{16}$ with a single exponential decay function fit (line). (c) Temperature-dependent photoluminescence spectra of $Rb_7Sb_3Cl_{16}$ powders. (d) The fitting results of FWHM as a function of temperature.

temperature range of 83–323 K to analyze the temperature-dependent PL spectra and the corresponding pseudocolor map is shown in Fig. S5 (online). Obviously, the integrated PL intensity monotonically increased as the sample was cooled down from 323 to 83 K. It is because the defect related nonradiative recombination was deactivated at low temperature. The integrated PL emission intensity ($I$) can be fitted by the following Eq. (2):

$$I(T) = \frac{I_0}{-1 + Ae^{-\frac{E_b}{k_B T}}}, \quad (2)$$

where $I_0$ and $I(T)$ are the PL intensity at 0 and $T$ K, respectively. $A$ is a constant, $E_b$ is the activation energy, or equivalently exciton binding energy, $k_B$ is Boltzman constant.

The fitting result based on the TDPL intensity with single exponential fitting showed that the photoluminescence activation energy of this material was 200 meV. Further, we have also studied the relation between FWHM and temperature (Fig. 3d). And the curve can be well fitted by a single configuration coordinate diagram [28]:

$$\mathrm{FWHM}(T) = 2.36\sqrt{S}\hbar\omega_{\mathrm{phonon}}\sqrt{\coth\frac{\hbar\omega_{\mathrm{phonon}}}{2k_B T}}, \quad (3)$$

where $S$ is the Huang-Rhys (HR) factor, $\hbar$ is the reduced Planck constant and $\omega_{\mathrm{phonon}}$ is the phonon frequency. The HR factor is associated with the displacement of the equilibrium positions of the nuclei upon exciting the chromophore, which reflects the strength of the linear electron-photon coupling [29]. And the larger the HR factor, the stronger the coupling, and the more likely STE is to occur. After applying this equation, the electron-phonon coupling parameter $S$ was obtained about 9.6, which is larger than the $CsPbBr_3$ ($S$ = 3.2) and $Cs_2NaYCl_6$ ($S$ = 7.0) [30,31]. This relatively large HR factor indicates a relatively strong electron-phonon coupling effect, which is necessary for the formation of self-trapped excitons. Further, we conducted the emission wavelength-dependent photoluminescence excitation measurements. As shown in Fig. 4a, the PLE spectra remained the identical shapes, which also suggested the emissions originated from the same excited state.

Our inorganic perovskite variant $Rb_7Sb_3Cl_{16}$ is expected to show good stability. We thus tested the water stability of $Rb_7Sb_3Cl_{16}$. It remained 80% of initial PL intensity after being immersed into water for 240 min (Figs. 4b and S6 (online)). Such good stability is still under question, and we suspect the main reason is the formation of $Sb_4O_5Cl_2$, the hydrolysis product, as the protection layer outside $Rb_7Sb_3Cl_{16}$ crystals. In order to verify our assumption, we carried out XRD measurements of the powder sample after soaking in deionized water for 3 h. The XRD results (Fig. S7 online) revealed the presence of $Sb_4O_5Cl_2$ (PDF No. 30-0091) [32]. As far as we know, $Rb_7Sb_3Cl_{16}$ shows the best water resistance ability among antimony-based perovskites [33–35].

Compared to other lead-free perovskites, our $Rb_7Sb_3Cl_{16}$ sample possesses a moderate PLQY with a broadband yellow emission (Fig. S1 and Table S3 online) and excellent stability, which is promising for lighting applications. Here, we manufactured warm-white LED by mixing our yellow phosphor with our home-made blue $Cs_2SnCl_6$:2.75%Bi to demonstrate their application [23]. $Rb_7Sb_3Cl_{16}$ and $Cs_2SnCl_6$:2.75%Bi were mixed within curable resin, coated on a commercial 365 nm LED chip and then excited by the LED chip, while the driving current is about 300 mA and voltage is about 3 V. As shown in the inset image in Fig. 5b, the working device based on the mixed phosphors emitted bright white light. The CIE coordinates of the emission output were

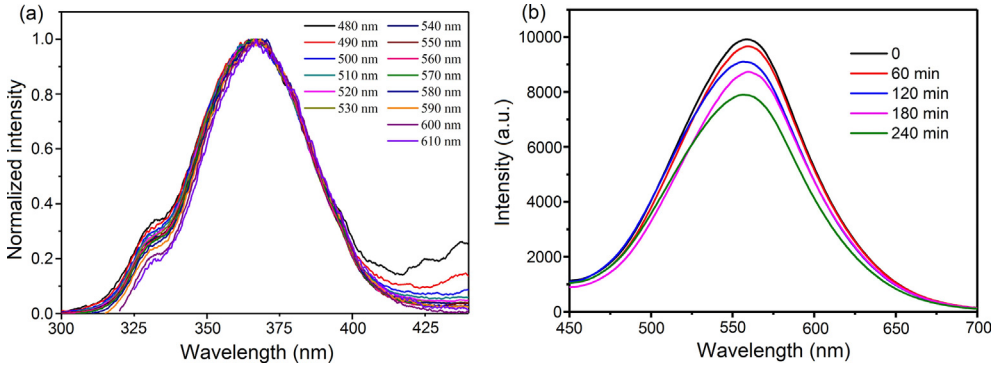


**Fig. 4.** (Color online) Photoproperties and water-stability of $Rb_7Sb_3Cl_{16}$. (a) Excitation spectra by monitoring different photoluminescence wavelength. (b) PL spectra of $Rb_7Sb_3Cl_{16}$ after immersion in deionized water for a specific period of time.

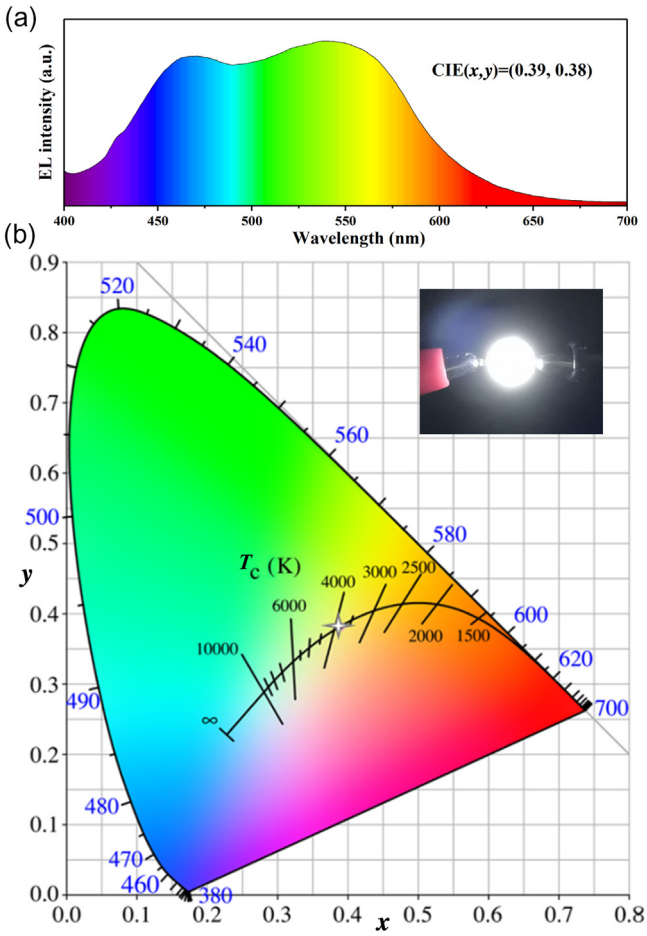


**Fig. 5.** (Color online) LED demo based on $Rb_7Sb_3Cl_{16}$ phosphor. (a) Luminescent spectra of warm-white emission LEDs based on $Rb_7Sb_3Cl_{16}$ phosphor. (b) CIE color coordinates corresponding to white-LED device and (inset) photo of an operating LED.

(0.39, 0.38), and the correlated color temperature was 3,986 K (Fig. 5).

## 4. Conclusions

In summary, we have reported antimony based $Rb_7Sb_3Cl_{16}$ perovskite variant with a yellow emission at 560 nm, a broad FWHM of 100 nm and a PLQY value of 26%. This perovskite variant demonstrated excellent water stability. Finally, by integrating this phosphor with our reported blue phosphor and 365 nm LED chip, we fabricated a warm-white LED. We believe our findings will promote further exploration of novel lead-free perovskite emitters.

## Conflict of interest

The authors declare that they have no conflict of interest.

## Acknowledgments

This work was supported by the National Key R&D Program of China (2016YFB0700702), the National Natural Science Foundation of China (51761145048, 61725401, and 51702107), China Postdoctoral Science Foundation (2018M632843), the Huazhong University of Science and Technology (HUST) Key Innovation Team for Interdisciplinary Promotion (2016JCTD111, 2017KFXKJC003), and Wuhan National High Magnetic Field Center. The authors thank the Analytical and Testing Center of HUST and the facility support of the Center for Nanoscale Characterization and Devices (CNCD), WNLO-HUST.

## Author contributions

Jiang Tang and Guangda Niu supervised the study. Zhifang Tan and Manchen Hu contributed to the synthesis and characterization of the materials, the PL measurements and analysis. Qingsong Hu contributed to the Rietveld refinement. Jinghui Li, Meiying Leng, and Liang Gao provided input to the data analysis and discussed the results. Guangda Niu, Zhifang Tan, and Manchen Hu wrote the manuscript. All authors assisted in manuscript preparation.

## Appendix A. Supplementary data

Supplementary data to this article can be found online at https://doi.org/10.1016/j.scib.2019.05.016.

## References

[1] Chin XY, Cortecchia D, Yin J, et al. Lead iodide perovskite light-emitting field-effect transistor. Nat Commun 2015;6:7383.
[2] Kim YH, Cho H, Heo JH, et al. Multicolored organic/inorganic hybrid perovskite light-emitting diodes. Adv Mater 2015;27:1248–54.
[3] Xing G, Mathews N, Lim SS, et al. Low-temperature solution-processed wavelength-tunable perovskites for lasing. Nat Mater 2014;13:476–80.
[4] Ling Y, Yuan Z, Tian Y, et al. Bright light-emitting diodes based on organometal halide perovskite nanoplatelets. Adv Mater 2016;28:305–11.
[5] Dai X, Zhang Z, Jin Y, et al. Solution-processed, high-performance light-emitting diodes based on quantum dots. Nature 2014;515:96.
[6] Zhou Q, Bai Z, Lu W, et al. In situ fabrication of halide perovskite nanocrystal-embedded polymer composite films with enhanced photoluminescence for display backlights. Adv Mater 2016;28:9163–8.

[7] Li X, Wu Y, Zhang S, et al. $CsPbX_3$ quantum dots for lighting and displays: room-temperature synthesis, photoluminescence superiorities, underlying origins and white light-emitting diodes. Adv Funct Mater 2016;26:2435–45.
[8] Jizhong S, Jianhai L, Xiaoming L, et al. Nanocrystals: quantum dot light-emitting diodes based on inorganic perovskite cesium lead halides ($CsPbX_3$) (adv Mater. 44/2015). Adv Mater 2015;27:7162–7.
[9] Lian Z, Yan Q, Lv Q, et al. High-performance planar-type photodetector on (100) facet of $MAPbI_3$ single crystal. Sci Rep 2015;5:16563.
[10] Pang S, Hu H, Zhang J, et al. $NH_2CHNH_2PbI_3$: an alternative organolead iodide perovskite sensitizer for mesoscopic solar cells. Chem Mater 2014;26:1485–91.
[11] Zhou Y, Garces HF, Padture NP. Challenges in the ambient raman spectroscopy characterization of methylammonium lead triiodide perovskite thin films. Front Opt 2016;9:81–6.
[12] Li Z, Hu Q, Tan Z, et al. Aqueous synthesis of lead halide perovskite nanocrystals with high water stability and bright photoluminescence. ACS Appl Mater Interfaces 2018;10:43915–22.
[13] Hu Q, Deng Z, Hu M, et al. X-ray scintillation in lead-free double perovskite crystals. Sci China Chem 2018;61:1581–6.
[14] Slavney AH, Leppert L, Saldivar Valdes A, et al. Small-band-gap halide double perovskites. Angew Chem Int Ed 2018;57:12765–70.
[15] Sun PP, Li QS, Yang LN, et al. Theoretical insights into a potential lead-free hybrid perovskite: substituting $Pb^{2+}$ with $Ge^{2+}$. Nanoscale 2015;8:1503.
[16] Hong WL, Huang YC, Chang CY, et al. Efficient low-temperature solution-processed lead-free perovskite infrared light-emitting diodes. Adv Mater 2016;28:8029–36.
[17] Hao F, Stoumpos CC, Cao DH, et al. Lead-free solid-state organic-inorganic halide perovskite solar cells. Nat Photon 2017;8:489–94.
[18] Luo J, Wang X, Li S, et al. Efficient and stable emission of warm-white light from lead-free halide double perovskites. Nature 2018;563:541–5.
[19] Yang B, Mao X, Hong F, et al. Lead-free direct band gap double-perovskite nanocrystals with bright dual-color emission. J Am Chem Soc 2018;140:17001–6.
[20] Xiao Z, Du KZ, Meng W, et al. Intrinsic instability of $Cs_2In(I)M(III)X_6$ (M=Bi, Sb; X = halogen) double perovskites: a combined density functional theory and experimental study. J Am Chem Soc 2017;139:6054.
[21] Hoefler SF, Trimmel G, Rath T. Progress on lead-free metal halide perovskites for photovoltaic applications: a review. Monatshefte Fur Chem 2017;148:795–826.
[22] Zhou C, Lin H, Tian Y, et al. Luminescent zero-dimensional organic metal halide hybrids with near-unity quantum efficiency. Chem Sci 2017;9:586–93.
[23] Tan Z, Li J, Zhang C, et al. Highly efficient blue-emitting Bi-doped $Cs_2SnCl_6$ perovskite variant: photoluminescence induced by impurity doping. Adv Funct Mater 2018;28:1801131.
[24] Garbout A, Bouattour S, Rego BAM, et al. Synthesis Raman and X-ray diffraction investigations of rubidium-doped $Gd_{1.8}Ti_2O_{6.7}$ pyrochlore oxide via a sol-gel process. J Crystal Growth 2007;304:374–82.
[25] Dohner ER, Hoke ET, Karunadasa HI. Self-assembly of broadband white-light emitters. J Am Chem Soc 2014;136:1718–21.
[26] Frank I, Hutter J, Marx D, et al. Molecular dynamics in low-spin excited states. J Chem Phys 1998;108:4060–9.
[27] Moreno M, Barriuso MT, Aramburu JA. The huang-rhys factor S(ALG) for transition-metal impurities: a microscopic insight. J Phys Conden Matter 1992;4:9481.
[28] Stadler W, Hofmann DM, Alt HC, et al. Optical investigations of defects in CD1-xznxte. Phys Rev B Conden Matter 1995;51:10619.
[29] Pieper J, Freiberg A. Electron-phonon and exciton-phonon coupling in light harvesting, insights from line-narrowing spectroscopies. In: Golbeck John, van der Est Art, editors. The Biophysics of Photosynthesis. New York, NY: Springer New York; 2014. p. 45–77.
[30] Lao XZ, Yang Z, Su ZC, et al. Luminescence and thermal behaviors of free and trapped excitons in cesium lead halide perovskite nanosheets. Nanoscale 2018;10:9949–56.
[31] Andrews LJ, Lempicki A, Mccollum BC, et al. Thermal quenching of chromium photoluminescence in ordered perovskites. I. Temperature dependence of spectra and lifetimes. Phys Rev B Condens Matter 1986;34:2735–40.
[32] Sarnstrand C. The crystal structure of antimony(III) chloride oxide $Sb_4O_5Cl_2$. Acta Crystallograph Sect B 1978;34:2402–7.
[33] Zhang J, Yang Y, Deng H, et al. High quantum yield blue emission from lead-free inorganic antimony halide perovskite colloidal quantum dots. ACS Nano 2017;11:9294–302.
[34] Egger DA. Intermediate bands in zero-dimensional antimony halide perovskites. J Phys Chem Lett 2018;9:4652–6.
[35] Han K, Zhang R, Mao X, et al. Air-stable, lead-free zero-dimensional mixed bismuth-antimony perovskite single crystals with ultrabroad band emission. Angew Chem 2019:2751–5.

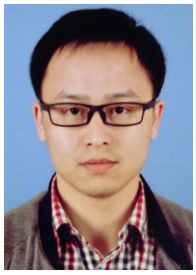

Zhifang Tan received his Master's degree from Huazhong Normal University at 2010, and his Ph.D. degree in Applied Chemistry from Hiroshima University at 2014. Now he works toward Postdoctor in Wuhan National Laboratory for Optoelectronics (WNLO). His research interest includes the research and exploration of photoelectric materials, lead or lead-free perovskite materials.

Jiang Tang received his Bachelor's degree from University of Science and Technology at 2003, and his Ph.D. degree in Materials Science and Engineering from University of Toronto at 2010. He spent one year and half as a postdoctoral researcher at IBM T. J. Watson research center and then joined in Wuhan National Laboratory for Optoelectronics, Huazhong University of Science and Technology as a professor in 2012. His group focuses on antimony selenide ($Sb_2Se_3$) thin film solar cells, halide perovskites nanocrystals for light emitting and single crystals for X-ray detection.